(Received 15 April 2025, Accepted 16 June 2025, Scheduled 25 June 2025)

Multi-Objective Optimization of Asymmetric Pole-Consequent Pole Permanent Magnet Motor

Jianwei Liang, Xinyu Zeng*, Yuqian Zhao, Tian Song, Xiubin Zhu, and Zhangsheng Liu

School of Electrical Engineering and Automation, Jiangxi University of Science and Technology, Ganzhou 341000, Jiangxi, China

ABSTRACT: This paper addresses the problem of sizeable cogging torque and torque ripple of conventional consequent pole permanent magnet (CPPM) motor and proposes an asymmetric pole-consequent pole permanent magnet (AP-CPPM) motor as a solution. A combined strategy of response surface method and multi-objective genetic algorithm is adopted. Firstly, sensitivity analysis of design variables and stratification were carried out, and subsequently the mathematical model between the design variables and optimization objective is obtained by Response Surface Methodology (RSM). Then, the high-sensitivity parameters are optimized using a Multi-Objective Genetic Algorithm (MOGA) to get the optimal solution. Finally, the electromagnetic performances of the motor before and after optimization are compared using Finite Element Analysis (FEA) software. The results indicated that the optimized motor reduced the torque ripple by 39.9% and the peak-to-peak value of cogging torque by 62.41% with only a 3.1% reduction in the output torque, which ensured good output characteristics and verified the feasibility of the optimization scheme.

1. INTRODUCTION

Permanent magnet synchronous motors are characterized by high performance and low losses, hence are widely used in electric vehicles, home appliances, ship propulsion, and other fields [1–4]. Most traditional permanent magnet motors use rare earth materials, which are limited resources, with their price constantly rising. Therefore, rare-earth-free or rare-earth-reduced permanent magnet motors have become one of the industry hotspots that scholars have been keen to study in recent years [5–7]. Among them, rare-earth-free permanent magnet motors have a lower power density and a limited range of applications because they do not use permanent magnets with high energy density. Less rare earth permanent magnet motor, represented by CPPM motor, has important research significance as it improves permanent magnet material's utilization rate to ensure the motor's high performance [8, 9].

Consequent pole structure, that is, the permanent magnet rotor (stator) polarity of the same or different permanent magnets with an iron core to replace the structure can not only save permanent magnet materials but improve the utilization of permanent magnets [10], but also ensures that the motor has a high torque density. However, since consequent pole permanent magnet structure exhibits an asymmetric air-gap magnetic field [11, 12], a large number of even-order harmonics exist in its air-gap magnet density, which leads to the problem of sizeable cogging torque and torque ripple, which in turn cause noise, vibration, and other issues [13], causing the motor to run unevenly. Therefore, how to reduce cogging torque has been a hot topic in the field of permanent magnet (PM) motors. Ref. [14] proposes a method to change the number of poles/slots, which can effectively solve the problem of consequent pole PM motors due to the even harmonics of the air gap flux density. However, there are situations that lead to an increase in torque ripple. Ref. [15] proposes slotting on surface-mounted of the motor permanent magnets to reduce cogging torque and rear earth material, and results show a 62% reduction in cogging torque and also a 6.7% reduction in rear earth material usage. Ref. [16] proposes N-S-Fe-S-N-Fe and Spoke-face-mounted hybrid pole novel rotor structures, which can effectively eliminate the torque ripple caused by the even harmonics of air gap magnet thus increasing the output torque of the motor and reducing torque ripple. However, there are also problems of complex structure and higher production costs. Ref. [17] proposes a method for cogging torque weakening based on pole arc width optimization for fractional slot cogging. This method attenuates the various harmonics of the cogging torque better than the conventional fractional slot method. The results show that the optimized cogging torque magnitude is reduced by 64% compared to the pre-optimization fractional slot method. Refs. [18, 19] propose a new method of auxiliary slots utilizing rectangular auxiliary slots on the rotor pole faces to reduce the cogging torque of the motor. The results show that the optimized motor cogging torque is reduced significantly. Ref. [20] uses the optimization of pole arc coefficients and rotor step skewing to weaken the cogging torque of a five-phase motor. The model with multiple optimization objectives is obtained using the response surface method, and the comparison results show that the harmonic distortion rate of the no-load reverse electromotive force of the motor is reduced by 27.88% and the cogging torque reduced by 79.52% after optimization. It is proved that the rotor step skewing can effectively weaken the cogging torque.

All of the above methods achieve cogging torque suppression, but a single method has some limitations. This paper

* Corresponding author: Xinyu Zeng (1071870144@qq.com).

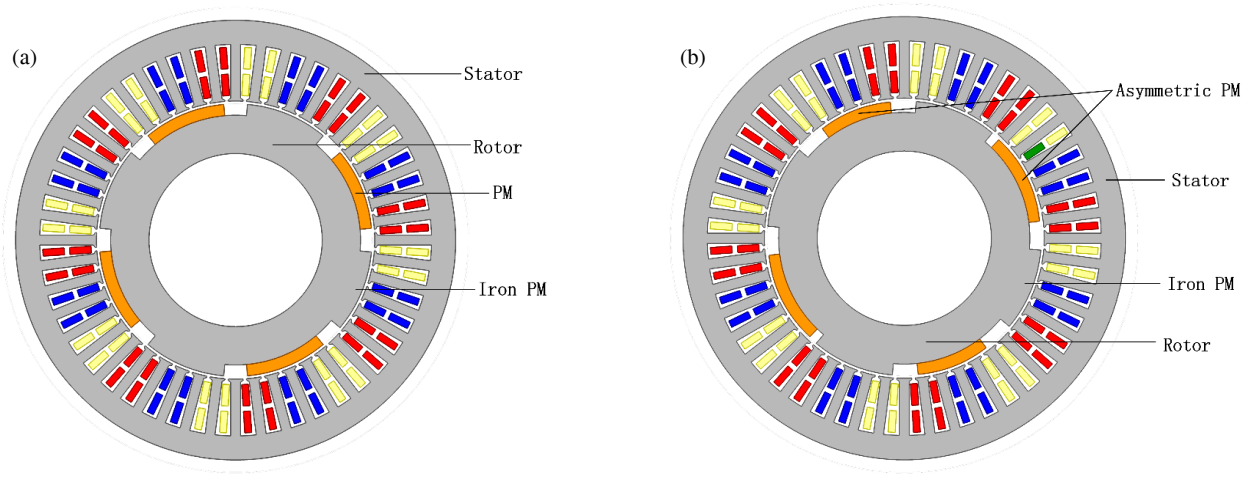

FIGURE 1. CPPM model. (a) Conventional. (b) Proposed.

proposes a 48-slot, 8-pole AP-CPPM utilizing the asymmetric structure (Including magnetic pole shifts, pole-arc coefficient changes, and unequal thicknesses) of the magnetic poles to solve the cogging torque problem caused by the CPPM structure. The motor parameters are also optimized by combining the response surface methodology with MOGA. Firstly, a comprehensive sensitivity analysis of design variables was conducted to stratify the strong and weak sensitivity parameters. Then, the response surface method established a mathematical model between the optimization parameters and objectives. Finally, the optimal optimization parameters were obtained by the MOGA, and conclusions were drawn.

2. CPPM MOTOR TOPOLOGY

The topology of a conventional CPPM motor, where the N (or S) pole is replaced by an iron core, is as shown in Fig. 1(a). Since half of the output torque reduces the amount of permanent magnets and remains almost the same in this motor compared to the conventional PM motor, the amount of PM used in the motor manufacturing process is reduced, thus lowering the manufacturing cost of the motor. However, CPPM motors tend to have large torque ripple and cogging torque, which in turn cause noise and vibration problems.

Cogging torque is generated by the interaction between the permanent magnets and stator core when the permanent magnet motor windings are not energized. The tangential component of the interaction force between the permanent magnets and armature teeth causes the cogging torque, which is expressed as:

$$T_{cog} = -\frac{\vartheta W}{\vartheta \alpha} \tag{1}$$

where W denotes the magnetic field energy of the motor in different energized states, and α denotes the position angle.

Assuming that the magnetic permeability of the iron core is infinity the magnetic field energy stored in the motor can be approximated as:

$$W \approx W_{airgap+PM} = \frac{2}{\mu_0}\int_V B^2 dV \tag{2}$$

where μ_0 is the vacuum permeability, and the distribution of the air gap permeability along the surface of the armature can be approximated as:

$$B(\theta,\alpha) = B_r(\theta)\frac{h_m(\theta)}{h_m(\theta)+\delta(\theta,\alpha)} \tag{3}$$

where $B_r(\theta)$, $\delta(\theta\alpha)$, and $h_m(\theta)$ are the distributions of permanent magnet remanent magnetization, effective air gap length, and permanent magnet magnetization direction length along the circumferential direction, respectively. Combining Equation (2) and Equation (3), W can be expressed as:

$$W = \frac{1}{2\mu_0}\int_V B_r^2(\theta)\left(\frac{h_m(\theta)}{h_m(\theta)+\delta(\theta,\alpha)}\right)^2 dV \tag{4}$$

where $B_r^2(\theta)$ can be expressed as:

$$B_r^2(\theta) = B_{r0} + \sum_{n=1}^{\infty} B_{rn}\cos 2np\theta \tag{5}$$

$B_{r0} = \alpha_p B_r^2$; $B_{rn} = \frac{2}{n\pi}B_r^2 \sin n\alpha_p\pi$, where p is the pole logarithm, and B_r is the residual magnetism of the permanent magnet

$$\left(\frac{h_m(\theta)}{h_m(\theta)+\delta(\theta,\alpha)}\right)^2 = G_0 + \sum_{n=1}^{\infty} G_n \cos q(\theta+\alpha) \tag{6}$$

α_p is the pole arc coefficient of the permanent magnet pole. The expression for the cogging torque can be obtained by bringing the obtained formula into Equation (1).

$$T_{cog(\alpha)} = \frac{\pi Z L_a}{4\mu_0}(R_2^2 - R_1^2)\sum_{n=1}^{\infty} nG_n B_{r\frac{nq}{2p}} \sin nq\alpha \tag{7}$$

where L_a is the axial length of the armature core; R_1 and R_2 are the outer diameter of the armature and inner diameter of the stator yoke, respectively; n is an integer such that $nq/2p$ is an integer.

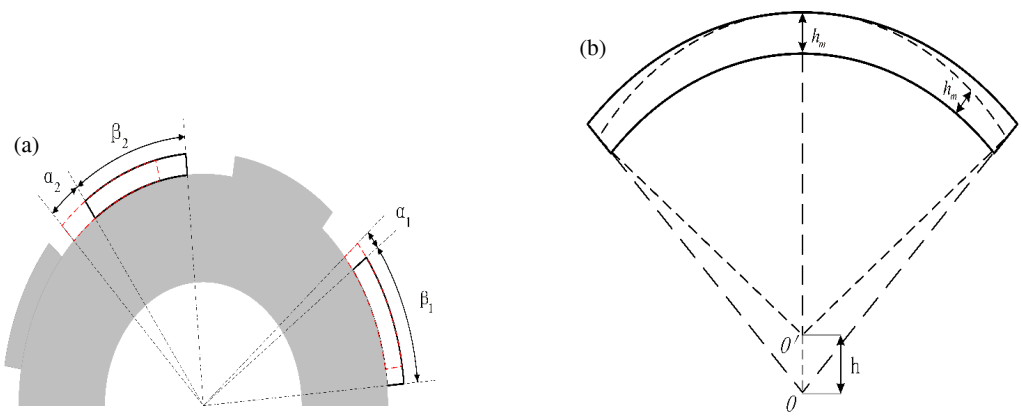

FIGURE 2. Asymmetrical construction. (a) Magnetic pole offset and magnetic Pole Arc Coefficients. (b) Unequal thickness of magnetic poles.

From the derivation, it can be seen that the amplitudes of B_{rn} and G_n directly affect the magnitude of the cogging torque. Changing the parameters of the magnetic poles can change the amplitude. Hence, we use the asymmetric structure optimization of the magnetic poles to reduce the cogging torque. Reducing the cogging torque to a certain extent will lead to a simultaneous reduction of the torque ripple.

The AP-CPPM motor proposed in this paper is shown in Fig. 1(b). The magnetic poles of this motor have two pairs (excluding the iron poles), which are divided into two combinations, with the neighboring poles in different groups. Asymmetric structure means (1) two combinations with unequal pole offset angles and (2) two combinations with unequal pole arc coefficients (one increasing and one decreasing). The structure is shown in Fig. 2(a), and all the magnetic poles are of unequal thickness, as shown in Fig. 2(b). The rest of the motor structure is consistent with the traditional model structure. The main structural parameters of the motor are shown in Table 1.

TABLE 1. CPPM main structural parameters.

parameters	value	unit
Number of slots	48	-
Number of poles	8	-
Outer radius of stator	155	mm
inner radius of stator	98	mm
inner radius of rotor	67	mm
Rated speed	1500	rpm
Air gap length	1	mm
PM materials	N35UH	-
Materials of stator and rotor	M470-50A	
Number of turns	5	-
PM thickness	4	mm
Axial length	9	mm

A single-parameter scan of the design variables gives the relationship between the different design variables and the optimization objective. As shown in Fig. 3, each design variable has a significant effect on the cogging torque verifying the correctness of the above derived equation (Since α_1 and α_2 single-parameter scans yield the same results, the α parameters are represented in a single plot. The same is true for β_1 and β_2). The change in the number of permanent magnets also results in changes in the average output torque. Multi-objective optimization is performed next in order to fully analyze the effect of design variables on parameters such as cogging torque.

3. MULTI-OBJECTIVE OPTIMIZATION

3.1. Optimization Process

First finite element software is used to establish the motor model. This paper uses five design variables, as shown in Table 2. Low torque ripple, low cogging torque, and high average out torque are selected as optimization objectives.

TABLE 2. Design variables and ranges.

Design Variable	Unit	Variation Ranges
α_1	deg	$-6 \sim 6$
α_2	deg	$-6 \sim 6$
β_1	deg	$36 \sim 41$
β_2	deg	$29 \sim 34$
h	mm	$2 \sim 10$

Sensitivity analysis and stratification of the design variables were also carried out, followed by modeling between the highly sensitive parameters and the optimization objectives using the RSM, and then the model was optimized using MOGA to obtain the candidate points. Finally, the correctness is verified by finite element simulation. The specific process is shown in Fig. 4.

3.2. Sensitivity Analysis

In optimal design, due to the large number of design variables, the degree of influence of different design variables on the optimization objective is not consistent, and scanning and analyzing all the variables at the same time will drastically increase the computation time for the optimal design. Parameter sensitivity can effectively analyze and evaluate the strength of the

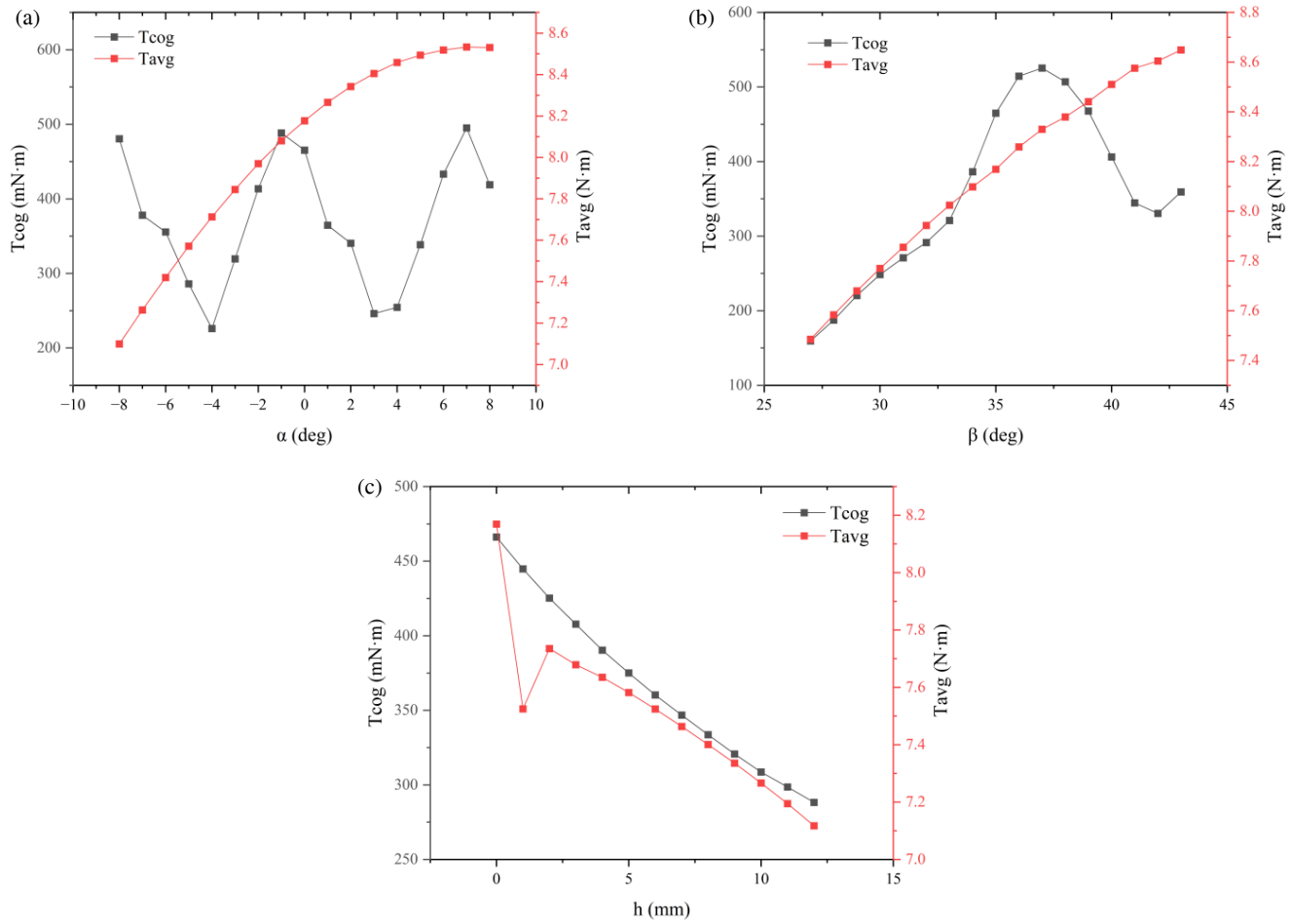

FIGURE 3. Single-parameter scanning. (a) Offset angle. (b) Magnetic pole angle (pole arc coefficients). (c) Eccentricity.

influence of design variables on the optimization objective and is considered to be one of the effective methods to achieve systematic and efficient optimal design [21]. The parameter sensitivity $S(x, y)$ of the design variable x to the optimization objective y is defined as follows:

$$S(x, y) = \frac{\text{cov}(x, y)}{\sigma_x \sigma_y} \tag{8}$$

$$\text{cov}(x, y) = \frac{\sum_{i=1}^{N} (x_i - x_m)(y_i - y_m)}{N} \tag{9}$$

where $\text{cov}(x, y)$ is the covariance; x_m and σ_x are the average value and standard deviation of the design variables x; y and σ_y are the average value and standard deviation of the optimization objective y; N is the sample space of the experimental design. According to Equation (8), the sensitivity magnitude of different design variables for different optimization objectives is calculated, as shown in Fig. 5. Usually, the greater the sensitivity is, the stronger the intrinsic connection is between the design variables and optimization objective. Positive sensitivity coefficients represent that the optimization objective will increase as the value of the design variable increases, and negative sensitivity coefficients show the opposite trend. Since each optimization parameter does not have a uniform effect on the optimization objective and considering the three optimization objectives, the weight coefficient method is used to evaluate each variable comprehensively. Therefore, this paper introduces an integrated sensitivity G, which can be described as:

$$G_{ni} = \lambda_T |S_T(x_i)| + \lambda_C |S_C(x_i)| + \lambda_R |S_R(x_i)| \tag{10}$$

$$\lambda_T + \lambda_C + \lambda_R = 1 \tag{11}$$

where λ_T, λ_C, and λ_R are the weighting coefficients of the average output torque, cogging torque, and torque ripple of the CPPM motor, respectively. $/S_{Y(x_i)}/$ is the absolute value of the sensitivity index of the design variable x with respect to the optimization objective y.

Since the final output performance of a motor is mainly indicated by the average output torque and torque ripple, the torque ripple should be minimized while maintaining the original average output torque. However, due to the problem of sizeable cogging torque in CPPM motors, the cogging torque needs to be minimized as much as possible. Therefore, the weight of both S_T and S_R is 0.35, and the weight of S_C is 0.3. This paper categorizes the design variables into high-level and low-level

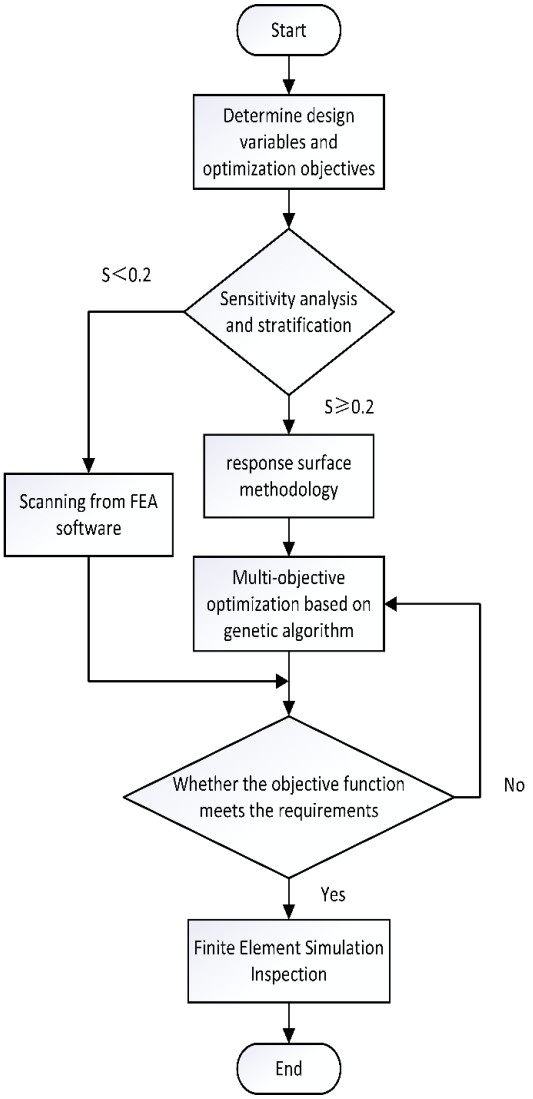

FIGURE 4. Optimization process of the motor.

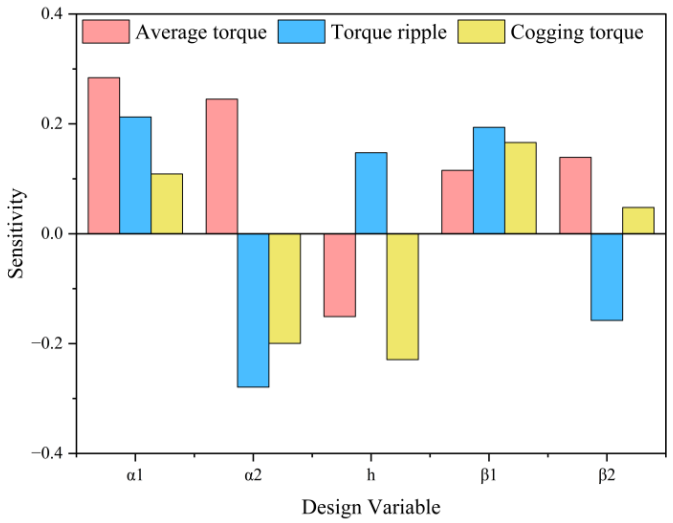

FIGURE 5. Sensitivity analysis chart.

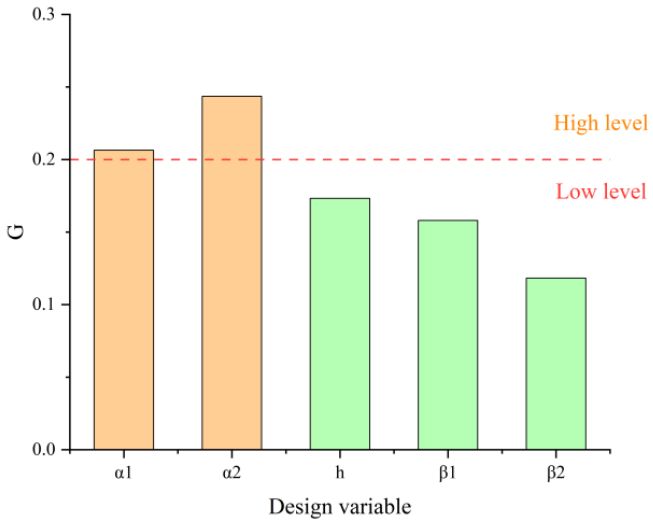

FIGURE 6. Integrated sensitivity.

variables as shown in Equation (12).

$$Range \cong \begin{cases} High-level, & Y \geq 0.2 \\ Low-level, & Y < 0.2 \end{cases} \tag{12}$$

From Fig. 6, it can be learned that the optimization parameters α_1 and α_2 belong to the high-level parameters, and β_1, β_2, and h belong to the low-level parameters after the calculation of the integrated sensitivity coefficients. For low-sensitivity parameters, choose to perform simulation analysis in finite element simulation and select the optimal simulation results as optimized values; for highly sensitive parameters, the algorithm optimization is continued.

3.3. Response Surface Creation

RSM is an integrated experimental design and optimization technique. Constructing a response surface model explores the complex relationship between multiple independent variables and dependent variables (response), and the optimal experimental conditions or parameter combinations are found accordingly. In this paper, the Latin hypercubic experimental design CCD (central composite design) method is used for samples to construct the response surface model between the design variables and optimization objective, and the mathematical relationship between the inputs and outputs is thus obtained.

$$y = a_0 + \sum_{i=1}^{3} a_i k_i + \sum_{i=1}^{3} a_{ii} k_i^2 \sum_{i=1}^{2} \sum_{j>1}^{3} a_i k_j + e_r \tag{13}$$

where y is the optimization objective, a the undetermined coefficient, k the optimization variable, and e_r the fitting error. Fig. 7 shows that α_1 and α_2 greatly influence the three optimization objectives. As shown in Fig. 7(a), the average output torque shows a monotonic relationship with α_1 and α_2. The output increases with the simultaneous increase of α_1 and α_2. From Fig. 7(b) and Fig. 7(c), we can see that the torque ripple and cogging torque are more complicated with α_1, α_2, and the model presents irregular graphs; therefore, after synthesizing the three response surface models, we can learn that the response points

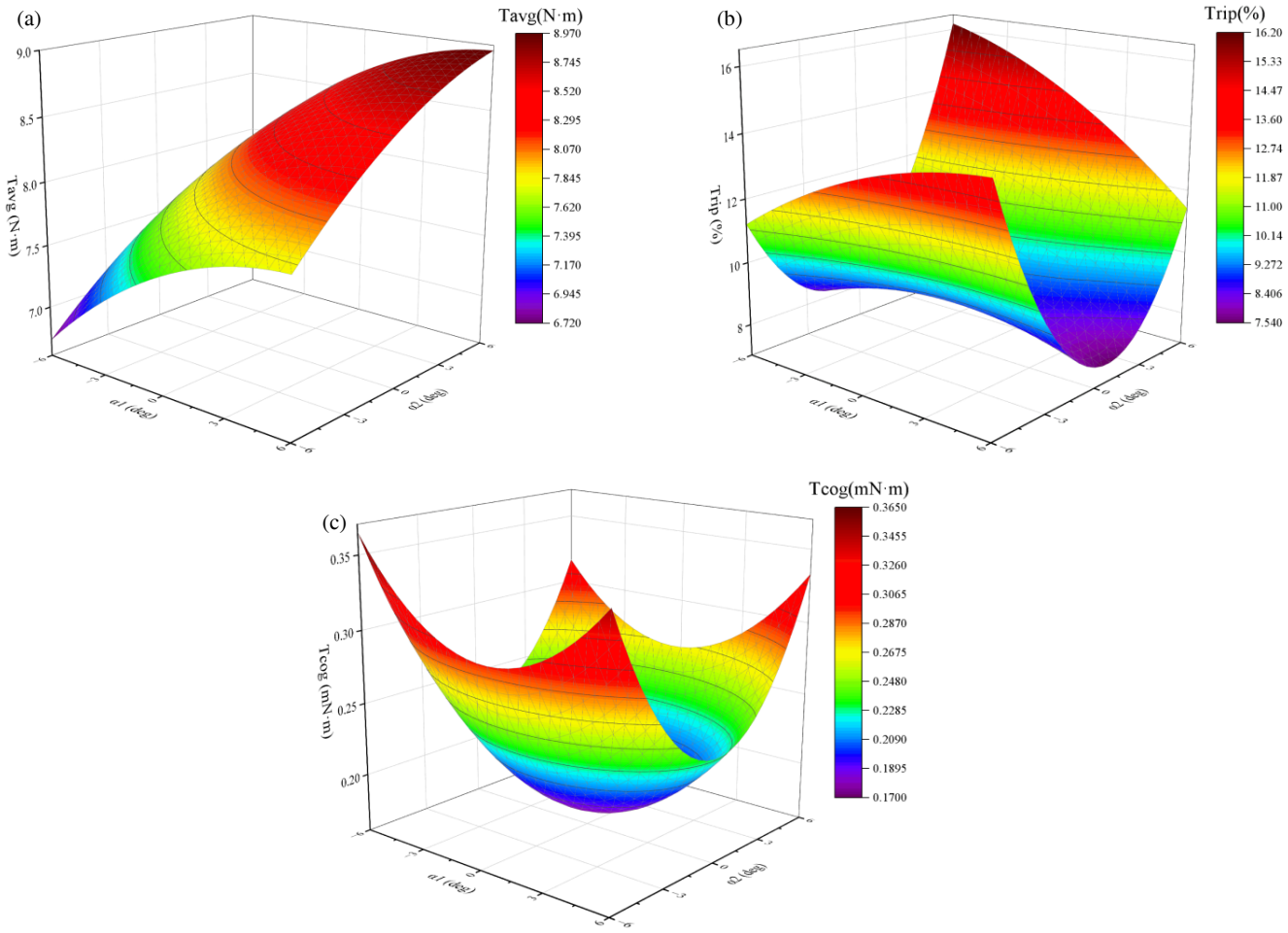

FIGURE 7. Response surface modeling between design variables and optimization objectives. (a) α_1 and α_2 to T_{avg} (b) α_1 and α_2 to T_{rip} (c) α_1 and α_2 to T_{cog}.

that satisfy the average output torque do not satisfy the other demands. When the average output torque is maximized, the torque ripple and cogging torque are large and do not meet the design requirements. In order to achieve the optimization goal better, further parameter optimization is needed to obtain better performance.

3.4. Multi-Objective Genetic Algorithm (MOGA)

MOGA method is a variant of the popular NSGA-II (Non-dominated Sorting Genetic Algorithm II) based on the concept of controlled elites. It is one of the most popular multi-objective genetic algorithms, which reduces the complexity of non-inferiority sorting genetic algorithms, has the advantages of fast running speed and good convergence of the solution set, and has thus become a benchmark for the performance of other multi-objective optimization algorithms. Multiple constraints and objectives can exist when finding the comprehensive optimal solution. In this study, MOGA is used to find the most suitable design variables to maximize the average output torque and minimize the cogging torque and torque ripple. The objective function is as follows:

$$\begin{cases} Obj: \begin{cases} Max\left(T_{avg}(z)\right) \\ Min\left(T_{cog}(z)\right) \\ Min\left(T_{rip}(z)\right) \end{cases} \\ s.t.: z_{\min} < z_k < z_{\max}\ (i = 1, 2, 3) \end{cases} \tag{14}$$

where maximum T_{avg}, minimum T_{rip}, and minimum T_{cog} are the optimization objectives. The iterative convergence process for the three optimization objectives is shown in Fig. 8. From Fig. 8(a), we know that the average output torque iteration is more stable and has gradually stabilized after the second time. From Fig. 8(b) and Fig. 8(c), we know that the torque ripple and cogging torque are gradually stabilized after many iterations; the torque ripple is not taken to be the minimum value; the low torque ripple candidates are discarded in order to achieve the optimization objective comprehensively. Eventually, after 9 iterations, the average output torque converged to approximately 8.03 N· m; torque ripple converged to approximately 8.68%; cogging torque converged to approximately 156.7 mN·m. The parameters before and after the optimization of the Design Variables are shown in Table 3.

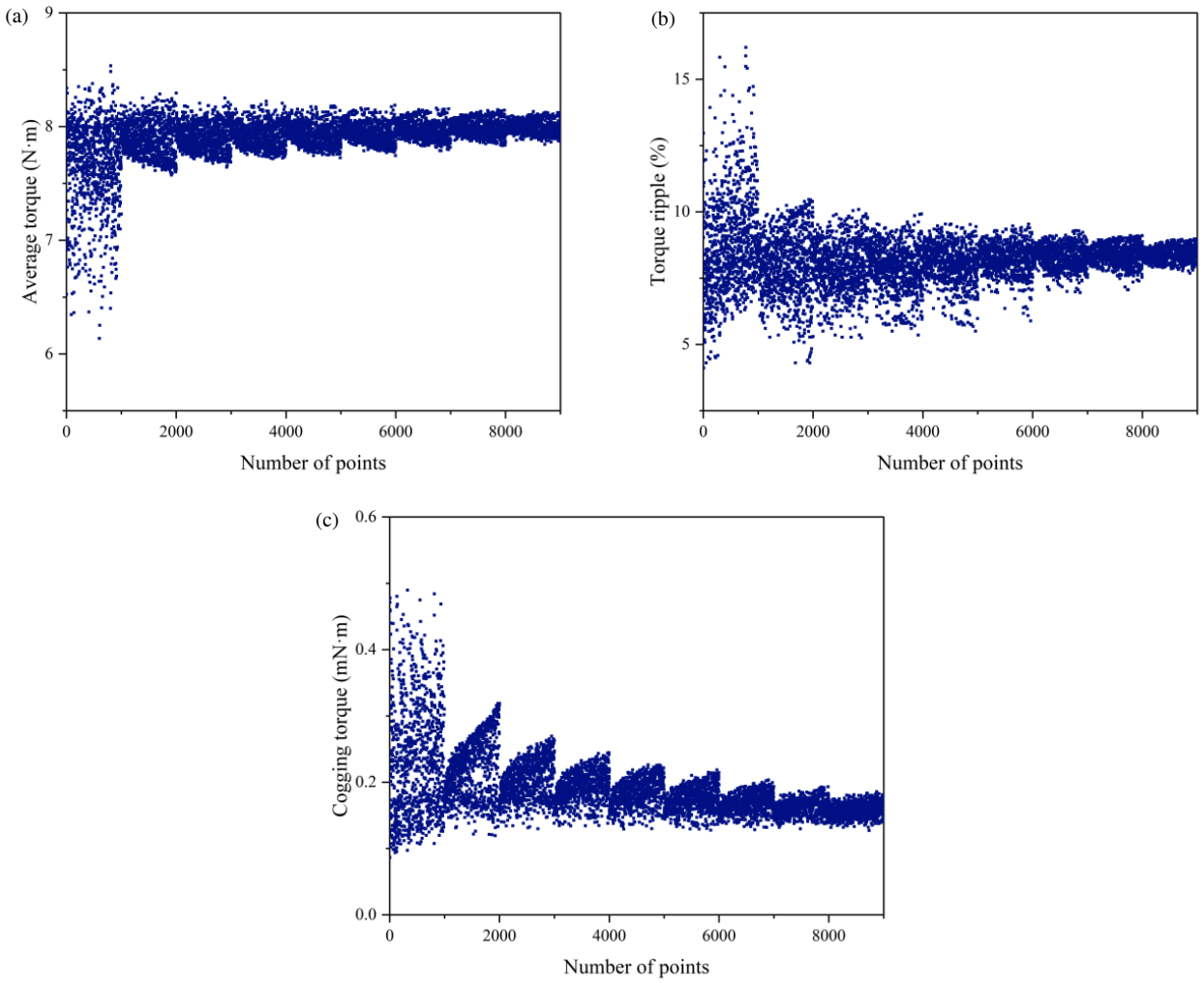

FIGURE 8. Convergence of the optimization objective. (a) T_{avg}. (b) T_{rip}. (c) T_{cog}.

TABLE 3. Initial and final values of design variables.

Parameter	Initial value	Optimal value
α_1 (deg)	c0	4.17
α_2 (deg)	0	−1.4
β_1 (deg)	35	39
β_2 (deg)	35	31
h (mm)	0	4

4. ELECTROMAGNETIC PERFORMANCE ANALYSIS

This paper establishes a traditional model in finite element software to analyze and compare with the optimized model to verify whether the optimized motor's performance has been improved. It mainly focuses on important parameters such as air gap magnetic density, no-load back-EMF, average output torque, cogging torque, and torque ripple.

4.1. Air-Gap Magnetic Density

The air gap flux density is shown in Fig. 9(a), and the air-gap flux density waveforms before and after optimization are slightly different because the pole shift affects the air-gap flux density. The Fourier decomposition analysis is shown in Fig. 9(b). Compared to the pre-optimization time, the base wave amplitude of the air-gap magnetic density is slightly reduced after optimization, and the base wave amplitude goes from 0.856 T before optimization to 0.837 T after optimization. Although the fundamental amplitude is slightly reduced and elevated fifth harmonic, the optimization suppresses the higher-order odd harmonics of the air-gap magnetism more significantly, where the 7th harmonic was reduced by 58.6%, the 9th harmonic by 59.4%, and the 11th harmonic by 56.7%; at the same time the even harmonics are attenuated to varying degrees except for the sixth and eighth. The reduction of harmonics favors the reduction of torque ripple.

4.2. No-Load BackEMF

The no-load back-EMF waveform is shown in Fig. 10(a) (Red is phase A, blue phase B, green phase C). The figure shows that there is a slight asymmetry in the optimized no-load back-EMF waveform, which is due to the asymmetric structure of the magnetic poles, but the optimized waveform is closer to a

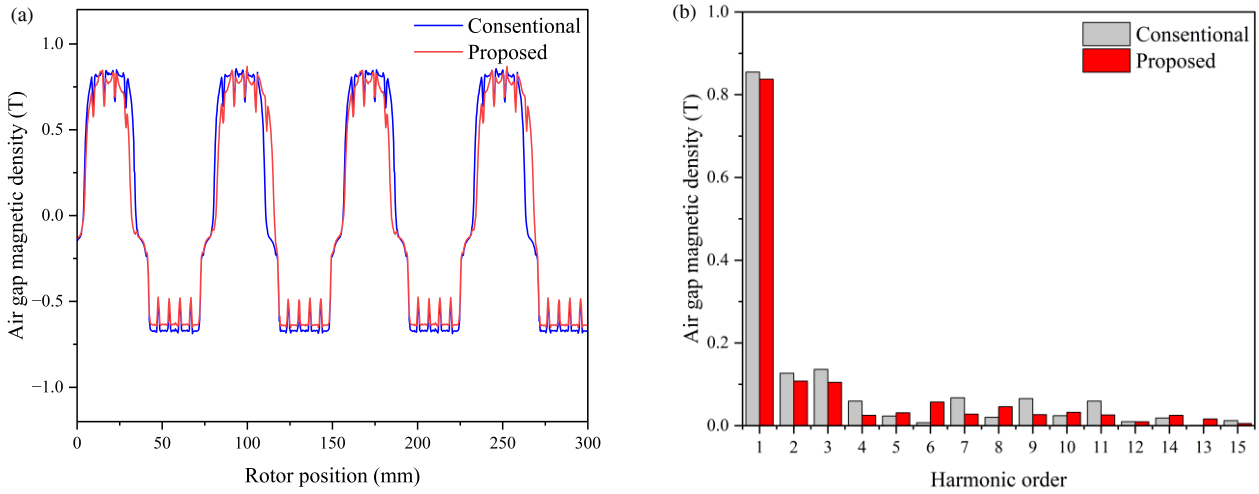

FIGURE 9. Air gap flux density. (a) Air gap flux density distribution. (b) Harmonic spectra.

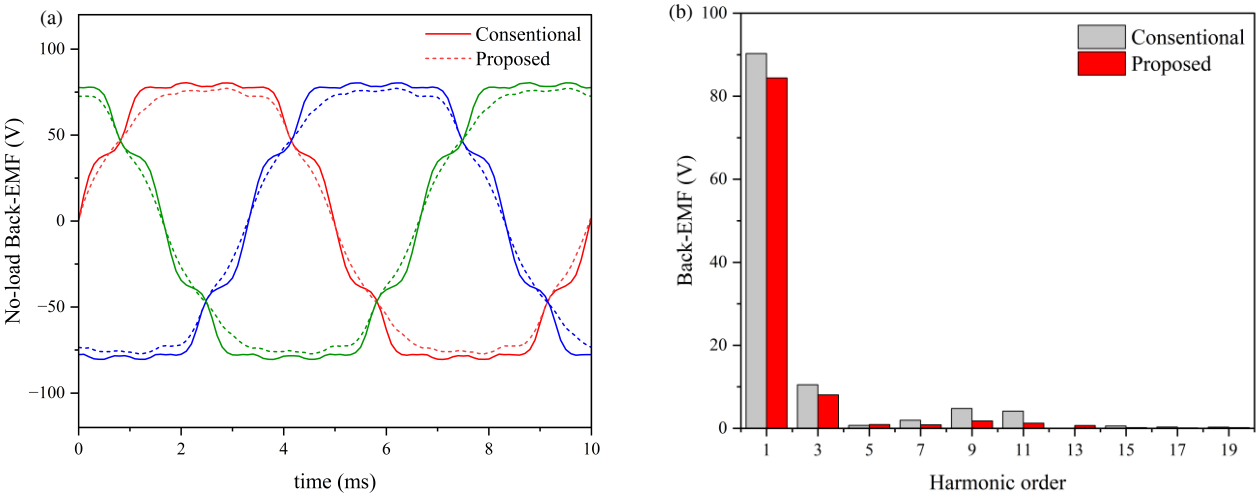

FIGURE 10. No-load BackEMF of CPPM machine. (a) Waveform. (b) Harmonic spectra.

sinusoidal waveform, and the curve is smoother, which is conducive to reducing the loss and vibration during the operation of the motor; therefore, a small-amplitude asymmetry in the waveform is acceptable. The Fourier decomposition of the no-load back-EMF is shown in Fig. 10(b), and the base wave amplitude of the A-phase no-load back-EMF of the permanent magnet motor before the optimization is 90.26 V. The base wave amplitude of the A-phase no-load back-EMF after optimization is 87.38 V, although it is reduced by about 3.2%. The optimized counter electromotive force's 7th, 9th, and 11th harmonics are weakened to different degrees. The 7th harmonic is reduced by 57.1%, the 9th harmonic by 62.9%, and the 11th harmonic by 69.8%. The optimized no-load back-EMF waveform distortion rate is reduced from 14.1% to 8.5%; the reduction in distortion rate will give a better sinusoidal nature to the reverse potential waveforms, improving the overall motor performance.

4.3. Torque Performance

In Fig. 11, the peak-to-peak value of optimized cogging torque has been significantly reduced from 930.64 mN·m to 349.81 mN·m, a reduction of 62.41%. In Fig. 12, the average output torque of the optimized motor is slightly reduced because the significant reduction in the cogging torque leads to a certain degree of reduction in the average output torque. The average output torque decreases from 8.16 N·m to 7.91 N·m, a decrease of 3.1%. In contrast, the fluctuation of the average output torque decreases dramatically, which proves that the optimized motor torque ripple is better optimized from 14.8% to 8.9%, a decrease of 39.9%. This also leads to a certain extent to the reduction of the average output torque. After the significant reduction of cogging torque and torque ripple, the average output torque is reduced by only 3.1%, which is an acceptable result, thus indicating that the proposed structure can achieve a more stable torque performance.

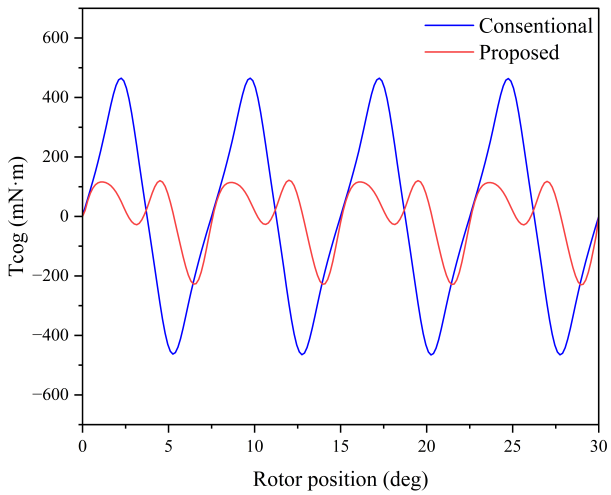

FIGURE 11. Cogging torque.

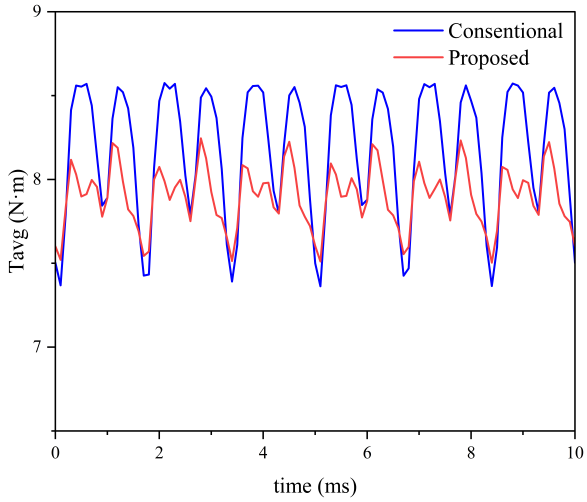

FIGURE 12. Average output torque.

5. CONCLUSION

This paper presents an AP-CPPM motor, and the optimum parameters for pole offset, eccentricity, and pole arc coefficients are determined by combining RSM and MOGA. The performance parameters of the motor before and after optimization were compared through finite element simulation, and the results of the comparison table show that the motor torque ripple suppression is evident under the premise that the average output torque is reduced by only 3.1%. The motor torque ripple decreased from 14.8% before optimization to 8.9% after optimization, thus giving a reduction of 39.9%. The peak-to-peak value of cogging torque has been dramatically reduced after optimization, from 930.64 mN to 349.81 mN, a reduction of 62.41%, which verifies the effectiveness of the optimized design.

REFERENCES

[1] Hwang, C.-C., S.-S. Hung, C.-T. Liu, and S.-P. Cheng, "Optimal design of a high speed SPM motor for machine tool applications," *IEEE Transactions on Magnetics*, Vol. 50, No. 1, 1–4, 2014.

[2] Du, G., C. Hu, Q. Zhou, W. Gao, and Q. Zhang, "Multi-objective optimization for outer rotor low-speed permanent magnet motor," *Applied Sciences*, Vol. 12, No. 16, 8113, 2022.

[3] Song, S.-W., M.-J. Jeong, K.-S. Kim, J. Lee, and W.-H. Kim, "A study on reducing eddy current loss of sleeve and improving torque density using ferrofluid of a surface permanent magnet synchronous motor," *IET Electric Power Applications*, Vol. 16, No. 4, 463–471, 2022.

[4] Bao, X., J. Liu, Y. Sun, and C. Wu, "Review and prospect of low-speed high-torque permanent magnet machines," *Transactions of China Electrotechnical Society*, Vol. 34, No. 6, 1148–1160, 2019.

[5] Boldea, I., L. N. Tutelea, L. Parsa, and D. Dorrell, "Automotive electric propulsion systems with reduced or no permanent magnets: An overview," *IEEE Transactions on Industrial Electronics*, Vol. 61, No. 10, 5696–5711, 2014.

[6] Du, Z. S. and T. A. Lipo, "Efficient utilization of rare earth permanent-magnet materials and torque ripple reduction in interior permanent-magnet machines," *IEEE Transactions on Industry Applications*, Vol. 53, No. 4, 3485–3495, 2017.

[7] Chung, S.-U., J.-W. Kim, Y.-D. Chun, B.-C. Woo, and D.-K. Hong, "Fractional slot concentrated winding PMSM with consequent pole rotor for a low-speed direct drive: Reduction of rare earth permanent magnet," *IEEE Transactions on Energy Conversion*, Vol. 30, No. 1, 103–109, 2015.

[8] Zheng, S., X. Zhu, Z. Xiang, L. Xu, L. Zhang, and C. H. T. Lee, "Technology trends, challenges, and opportunities of reduced-rare-earth PM motor for modern electric vehicles," *Green Energy and Intelligent Transportation*, Vol. 1, No. 1, 100012, 2022.

[9] Li, J., K. Wang, F. Li, S. S. Zhu, and C. Liu, "Elimination of even-order harmonics and unipolar leakage flux in consequent-pole PM machines by employing NS-iron–SN-iron rotor," *IEEE Transactions on Industrial Electronics*, Vol. 66, No. 3, 1736–1747, 2019.

[10] Li, J. and K. Wang, "A parallel hybrid excited machine using consequent pole rotor and AC field winding," *IEEE Transactions on Magnetics*, Vol. 55, No. 6, 1–5, 2019.

[11] Chung, S.-U., J.-W. Kim, B.-C. Woo, D.-K. Hong, J.-Y. Lee, and D.-H. Koo, "A novel design of modular three-phase permanent magnet vernier machine with consequent pole rotor," *IEEE Transactions on Magnetics*, Vol. 47, No. 10, 4215–4218, 2011.

[12] Li, F., K. Wang, J. Li, and H. J. Zhang, "Suppression of even-order harmonics and torque ripple in outer rotor consequent-pole PM machine by multilayer winding," *IEEE Transactions on Magnetics*, Vol. 54, No. 11, 1–5, 2018.

[13] Fei, Q., Y. Deng, H. Li, J. Liu, and M. Shao, "Speed ripple minimization of permanent magnet synchronous motor based on model predictive and iterative learning controls," *IEEE Access*, Vol. 7, 31 791–31 800, 2019.

[14] Li, F., K. Wang, P. Gao, S. Zhu, C. Liu, and R. Jiang, "Investigation of cogging torque and torque ripple in consequent Pole permanent magnet machine with different slot/pole number combinations," *Proceedings of the Chinese Society of Electrical Engineering*, Vol. 42, No. 17, 6491–6498, 2022.

[15] Yu, H.-C., B.-S. Yu, J.-T. Yu, and C.-K. Lin, "A dual notched design of radial-flux permanent magnet motors with low cogging torque and rare earth material," *IEEE Transactions on Magnetics*, Vol. 50, No. 11, 1–4, 2014.

[16] Wang, K., J. Li, S. S. Zhu, and C. Liu, "Novel hybrid-pole rotors for consequent-pole PM machines without unipolar leak-

age flux," *IEEE Transactions on Industrial Electronics*, Vol. 66, No. 9, 6811–6823, 2019.

[17] Li, Q. and M. Dou, "A cogging torque reducing method of fractional-slot in brushless DC motors," *Small and Special Electrical Machines*, Vol. 40, No. 3, 31–33, 2012.

[18] Yang, Y., X. Wang, and T. Ding, "Method of reducing cogging torque of solid-rotor permanent magnet synchronous motors," *Electric Machines and Control*, Vol. 12, No. 5, 520–523, 2008.

[19] Xu, X., X. Zhang, P. Wang, C. Wang, and X. Li, "A method for weakening cogging torque of interior permanent magnet synchronous motor in electric vehicle," *China Science Paper*, Vol. 15, No. 8, 942–947, 2020.

[20] Gao, M., X. Yang, S. Jiang, B. Tian, S. Zhao, J. Cao, and Z. Zhang, "The method for reducing cogging torque by suitable selection of the pole-arc coefficient and rotor step skewing in five-phase permanent magnet motor," *Proceedings of the Chinese Society of Electrical Engineering*, Vol. 43, No. 22, 8922–8935, 2023.

[21] Xie, B., Y. Zhang, Z. Xu, F. Zhang, and W. Liu, "Review on multidisciplinary optimization key technology of electrical machine based on surrogate models," *Transactions of China Electrotechnical Society*, Vol. 37, No. 20, 5117–5143, 2022.